NASA Technical Paper 1327

Discrimination of Rock Classes and Alteration Products in Southwestern Saudi Arabia With Computer-Enhanced Landsat Data

H. W. Blodget, F. J. Gunther,
and M. H. Podwysocki

OCTOBER 1978

NASA

NASA Technical Paper 1327

Discrimination of Rock Classes and Alteration Products in Southwestern Saudi Arabia With Computer-Enhanced Landsat Data

H. W. Blodget
Goddard Space Flight Center, Greenbelt, Maryland

F. J. Gunther
Computer Sciences Corporation, Silver Spring, Maryland

M. H. Podwysocki
Goddard Space Flight Center, Greenbelt, Maryland

This document makes use of international metric units according to the Systeme International d'Unites (SI). In certain cases, utility requires the retention of other systems of units in addition to the SI units. The conventional units stated in parentheses following the computed SI equivalents are the basis of the measurements and calculations reported.

ABSTRACT

Digital Landsat MSS data for an area in the southwestern Arabian Shield
have been computer-enhanced to improve discrimination of rock classes,
and recognition of gossans associated with massive sulphide deposits.

The test area is underlain by metamorphic rocks that are locally intruded
by granites; these are partly overlain by sandstones. The test area further
includes the Wadi Wassat and Wadi Qatan massive sulphide deposits, which
are commonly capped by gossans of ferric oxides, silica, and carbonates.

Color patterns and boundaries on contrast-stretched ratio color composite
imagery, and on complementary images constructed using principal com-
ponent and canonical analyses transformations, correspond exceptionally
well to 1:100,000 scale field maps. A qualitative visual comparison of in-
formation content showed that the ratio enhancement provided the best
overall image for identification of rock type and alteration products.

CONTENTS

DISCRIMINATION OF ROCK CLASSES AND ALTERATION PRODUCTS IN SOUTHWESTERN SAUDI ARABIA WITH COMPUTER-ENHANCED LANDSAT DATA

H. W. Blodget*
F. J. Gunther†
M. H. Podwysocki‡
Goddard Space Flight Center
Greenbelt, Maryland

INTRODUCTION

Discrimination among rock classes on the basis of gray tone or color, texture, and shape has traditionally posed a problem to the photogeologist. This problem becomes increasingly severe with satellite imagery because of the significant decrease in resolution.

The availability of digital multispectral scanner (MSS) data from the Landsat satellite has led to the development of computer algorithms applicable to information enhancement in many fields. For example, agricultural surveys, land-cover assessment and change monitoring, and hydrologic flood modeling can be accomplished rapidly, on a regional basis, and with a high degree of accuracy.

Based on such experience in these nongeologic disciplines, it was logical to assume that existing computer programs could be modified or that new algorithms could be developed that would aid the geologist/interpreter in identifying rock types. The objective was to assess several of the more promising digital techniques, using an "idealized" geological test site. The main effort was placed on using the facilities available at the Goddard Space Flight Center (GSFC), and emphasis stressed the capabilities of VICAR/SMIPS (a GSFC version of an image processing system originated at the Jet Propulsion Laboratory) and the Pennsylvania State University, Office of Remote Sensing of Earth Resources (ORSER) systems.

Because many variable surface characteristics affect the response of an electromagnetic sensor, selection of an appropriate geologic test site required the consideration of a number

---

*NASA/Goddard Space Flight Center, Greenbelt, Maryland 20771.
†Computer Sciences Corporation, Silver Spring, Maryland 20910.
‡NASA/Goddard Space Flight Center (present address: U.S. Geological Survey, Reston, Virginia 22092).

of primary factors. Among these were the atmosphere, vegetative cover, soil, topography, and bedrock lithology. To evaluate the rock-discrimination capabilities of the various computer algorithms in a situation having the fewest of these variables, a test area in the southern Arabian Shield was selected for study (figure 1). This area contains a wide variety of rock types that are generally well-exposed, unweathered, and practically free of vegetation. The area has also been well-mapped at the reconnaissance level. It includes many outcrop areas that are large and homogeneous enough for low-resolution study and that can be readily located on Landsat imagery. Furthermore, although the Arabian Highlands appear to be remote and inaccessible, the area is being re-mapped by the U.S. Geological Survey in cooperation with the government of Saudi Arabia. Thus, geologic interpretations could be field-evaluated, and the data could be incorporated into an active geological mapping program.

REGIONAL ENVIRONMENT AND GEOLOGY

This low-latitude desert test area is located in the Eastern Asir Mountains, about 100 kilometers (60 miles) north of Najran on the Yemen Arab Republic border. The highly dissected terrain, generally underlain by metamorphic rocks, is moderately rugged, and local relief exceeds 500 meters. Localized areas of low relief, however, are frequently developed over igneous intrusives because of their relatively rapid mechanical degradation (figure 2). These so-called "cookie-cutter" granite intrusions vividly demonstrate the dominance of mechanical weathering processes in this arid environment.

The test area is on the southeastern margin of the Arabian Shield. The basement rocks consist of a complex sequence of generally metamorphosed, interlayered volcanic and sedimentary Precambrian assemblages. These are locally intruded by igneous rocks ranging in composition from gabbro to syenite and in age from Precambrian to Cambrian (?). The volcanic rocks in the area vary in composition from andesite to rhyolite and in texture from agglomerate to thick, massive flows and lithic tuff. They are commonly interlayered with sedimentary strata that variously include sandstone, conglomerate, graywacke, shale, and limestone. The basement rocks are, in part, unconformably overlain by recent unconsolidated alluvial and aeolian sands and Cambro-Ordovician Wajid sandstone. The latter laps onto the shield from the east and south. This sandstone has been eroded from much of the western part of the test area and is now commonly observed only on isolated buttes where the remnants cap the basement (figure 3).

The test area also includes the Wadi Wassat and Wadi Qatan (Adhbat) massive sulphide deposits, which are among the largest areas of metallic mineralization known on the entire Arabian Peninsula. They extend over a length of several tens of kilometers and occur as stratabound lenses within metavolcanic rocks. Mineralization occurs mainly as metamorphosed syngenetic deposits and is made up largely of very fine-grained massive and disseminated sulphides that consist primarily of pyrite and pyrrhotite; chalcopyrite and sphalerite are
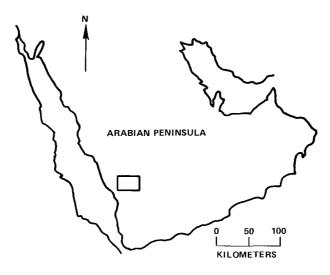
2

Figure 1. Index map Wadi Wassat test site.

Figure 2.   Wind erosion of a coarse-crystalline granite. Note the different erosional pattern exhibited by the metamorphic rocks below the horizon. Rapid mechanical degradation of granites in this area commonly forms circular areas of low relief within the terrain composed of metamorphic rocks.
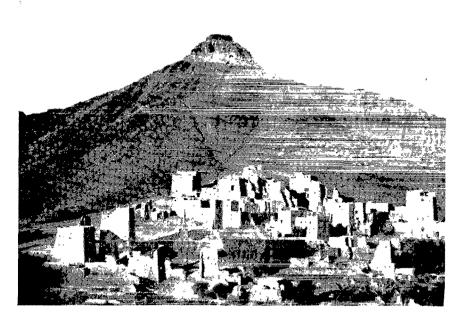
Figure 3. Wajid sandstone capping metamorphic rocks north of the village of Zahran.

present in subcommercial quantities. These mineralized zones are commonly capped by gossans consisting of brown, buff, or maroon mixtures of ferric oxides, silica, and carbonate. The major gossans were initially described by G. F. Brown in 1952 in conjunction with a regional reconnaissance geologic mapping program (Reference 1) and were subsequently mapped in greater detail by Weissenborn and Earhart (Reference 2), Overstreet and Rossman (Reference 3), Jackaman (Reference 1), and Dodge and Rossman (Reference 4). Greenwood* has more recently incorporated this detailed gossan outcrop data into his revision of the 30 by 30 minute, 1:100,000 geologic map of the Wadi Wassat Quadrangle.

APPROACH

Since digital Landsat scanner data first became available, there has been a small but expanding effort to develop computer algorithms that permit more certain identification of materials at the Earth's surface. These research efforts can be divided into two categories: thematic classification and image enhancement.

---

*W. R. Greenwood, Reconnaissance geology of the Wadi Wassat quadrangle, Kingdom of Saudi Arabia, Scale 1:100,000 (in press).

4

Computer classification, which attempts to isolate specific categories of materials based on measurable physical parameters (i.e., the digital spectral numbers associated with that material) that are meaningful to a specific user, is based on rigorous statistical procedures. As noted earlier, such programs have been successfully applied in several discipline areas. In geology, however, classification routines have generally been less successful (Reference 5).

Computer classification of rock and soils can be accomplished with some accuracy in areas in which vegetation and topographic relief is minimal. Materials within this class include alluvium, many broad-beach deposits, and some fresh extrusives (Reference 5). In highly dissected terrain, however, the spectral reflectance values tend to vary considerably between pixels, and it is extremely difficult to adequately define the computer training sites required for all classification procedures. This variation is primarily caused by shadows and slopes, which can modify spectral reflectance values within homogeneous materials. A single rock type can thus exhibit a range of spectral reflectance that varies with the illumination of the reflecting surface.

CONTRAST-STRETCHED RATIO ENHANCEMENT

The beginning of this work involved evaluating image-enhancement techniques that would minimize the effects of topography. The initial efforts utilized selected programs in the VICAR/SMIPS system and extended the initial concepts described by Rowan et al. (Reference 6) and Goetz et al. (Reference 7). Several algorithms in this system improved the rock-discrimination capability of the basic digital Landsat data; however, the one that appeared to be most applicable for the test area combined three sets of contrast-enhanced ratio data into a color-composite image. In brief form, this procedure consisted of three fundamental steps: (1) ratio values were obtained by dividing the spectral values for two MSS bands on a pixel-by-pixel basis; (2) the resultant data were rescaled so that they filled the entire dynamic range of the display medium; and (3) the stretched data derived from the three ratio sets were combined into color-composite imagery using various combinations of filters and light intensities. This procedure is useful because the ratio values, determined by combining data from MSS band pairs, tend to remove first-order brightness differences attributable to topography. In addition, the ratio data tend to normalize the response of similar materials having similar spectral response curves but varying albedos; they also display the slope of the reflectance spectrum of a material between two bands on a single black-and-white image.* Because the simple ratios derived with this algorithm generally show a narrow range of values, the data must be contrast-enhanced before image construction to attain optimum display characteristics. A number of contrast-enhancement algorithms are available, and several of the more important ones are discussed by Goetz et al. (Reference 7, page 107). The ramp cummulative distribution function (CDF) contrast stretch proved to be most useful for rock discrimination.
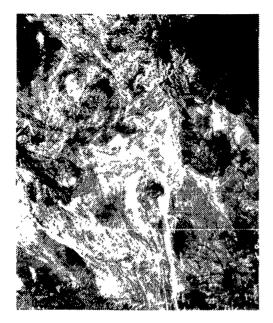
---

*B. S. Siegel, and A. R. Gillespie, *Remote Sensing in Geology*, John Wiley and Sons, Inc., New York (in press).
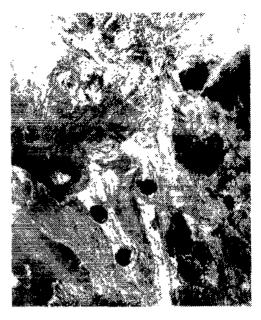
It should be noted, however, that the suppression of albedo by ratio processing can also occasionally cause items that are easily separable on standard imagery to become inseparable on the ratio image, particularly if materials have similar spectral-reflectivity slopes, such as alluvium adjacent to its provenance. It is, therefore, strongly recommended that both ratio and nonratio image formats be used in concert for geological interpretation.

Experience has shown that three contrast-stretched ratio images (figure 4) of a possible twelve ratio combinations have the greatest visible rock-discrimination capability in the arid areas of the Arabian Shield (Reference 5). The extremes of the gray scale for these images represent the largest spectral-reflectivity differences. Thus, the lightest areas in each ratio image are those for which the numerator of the ratio is greater than the denominator; note that the granites (gr) tend to be light in the MSS-4/5 image indicating that the reflectance of granite in MSS band 4 is considerably higher than that in band 5. In the MSS-6/7 image, however, the granites are dark, indicating a higher reflectance value for granite on band MSS-7 than on MSS-6.

In certain aeolian sediments (E), the relative tonal and spectral values are reversed, indicating that MSS-5 reflectance is greater than that of MSS-4, that of MSS-6 is greater than that of MSS-5, and that of MSS-7 is greater than that of MSS-6. A distinctive muscovite granite (M) is moderately dark in all three images. The interband relationships are reversed for amphibolites (a), which are light on each of the three images. However, the latter cannot be visually distinguished from metavolcanics (bu) or certain alluvial sediments (A) solely on the basis of tone. The Wadi Wassat gossan (Gs, note small arrow) can be located on the MSS-4/5 and MSS-5/6 images, but does not have a unique gray tone. The MSS-6/7 gossan ratio value is too similar to that of the metavolcanic host rock for visual separation to be made. From even these few examples, it is clear that greater distinction among rock classes is possible with black and white ratio images than with standard Landsat MSS band imagery (figure 5). The information content of these enhanced-ratio images still has severe limitations, and numerous ambiguities exist. The ability to distinguish among different surface materials, however, can be significantly further increased by selectively combining the same ratio data sets into a color-composite image. This increase is possible for two primary reasons: (1) because information from three ratio data sets is combined, and (2) even more important, because the color created by the compositing process permits a wider range of visual discrimination. This occurs because the normal human eye can separate more than 100 times more color combinations than gray-scale values (Reference 8).

A large number of color-filter, ratio, and stretch combinations are available for use in creating a variety of color-composite images. The best combination for rock discrimination in the Arabian Shield combined the three ratio combinations described previously into a color-ratio composite image; the MSS-4/5 ratio data were passed through a blue filter, whereas the 5/6 and 6/7 values were projected through green and red filters, respectively (Reference 5). The resultant ratio composite made from this combination is shown in figure 6.

6

MSS-4/5

MSS-6/7

MMS-5/6

LEGEND

A	ALLUVIUM
a	AMPHIBOLITE
E	AEOLIAN SAND
gp	GRANITE
Gs	GOSSAN
M	MUSCOVITE GRANITE
bu	METAVOLCANICS

N

0   10   20   30   40   50
KILOMETERS
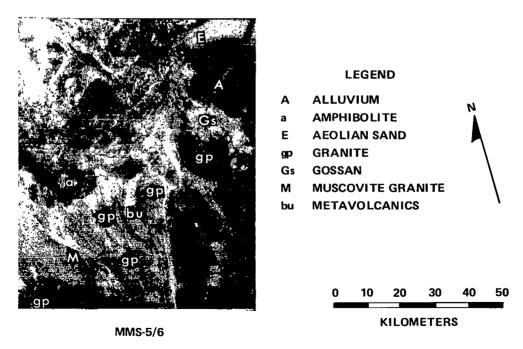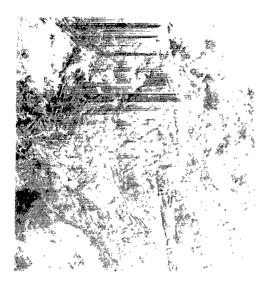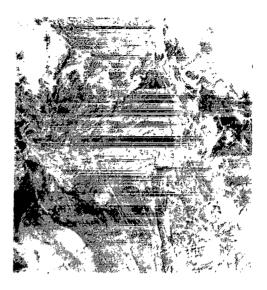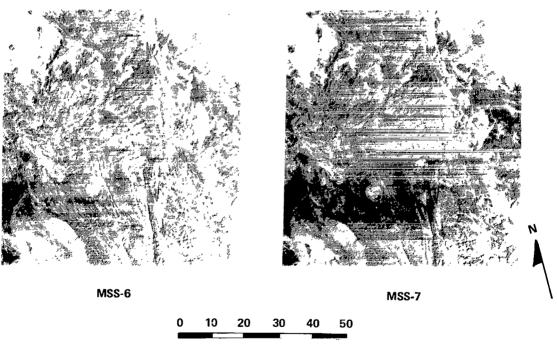
Figure 4. Landsat contrast-enhanced ratio images of the Wadi Wassat area
(southeast corner of scene 1226-07011).

MSS-4

MSS-5

MSS-6

MSS-7

N

0   10   20   30   40   50

KILOMETERS

Figure 5. Standard Landsat imagery taken from the southeast corner of scene 1226-07011.
The area is approximately the same as that shown on figure 4.

GEOLOGIC ANALYSIS OF CONTRAST-STRETCHED RATIO COLOR-COMPOSITE IMAGERY

The ratio-composite image was first analyzed by studying the two published regional geologic maps available for the area. These included the 1:500,000-scale reconnaissance mapping of the Asir Quadrangle (figure 7) (Reference 9), and the 1:100,000-scale reconnaissance geologic map of the Wadi Wassat Quadrangle (Reference 3, Plate 1). The latter provided considerably more detailed information, and had supporting textual material to complement the geologic map. Later, W. R. Greenwood generously provided prepublication 1:100,000-scale drafts of his two geologic maps that included much of the test area. The first of these was a geologic revision of the Wadi Wassat Quadrangle; the second, the Malahah quadrangle, showed the geology immediately to the west. Both maps incorporated the work of earlier geologists. Greenwood was fortunate to have had extensive helicopter support for his mapping program, and his entire quadrangle area was readily accessible for field study. Thus, although Greenwood considered these maps to be officially preliminary, they proved to be the most useful and accurate references available for defining the surface geology in our study area.

The prime objective of this comparative study was to identify the mapped rock units that could be correlated with multispectral ratio data expressed as unique color signatures on the ratio-composite image; conversely, it was then possible to locate the remaining problem areas in which correlations were ambiguous or nonexistant. The geology in some of these enigmatic areas could then be more clearly defined using alternative enhancement procedures, but absolute clarification required additional field study. After all of the possible spectrally defined rock units had been visually identified, the enhanced image was used to extend and/ or improve regional stratigraphic correlations into more poorly mapped areas (Greenwood, private communication, 1976).

Figure 7 is a geologic map modified from that portion of the Asir Quadrangle (1:500,000) covering the area of the ratio color-composite image (figure 6). The three dark-blue subcircular spectral units just south of the center of figure 6 correspond closely with the peralkalic granite intrusions (gp) identified on figure 7. In addition, all other (gp) intrusions that are mapped in the lower two-thirds of the test area can be identified equally well. In the northern part of the scene, however, similar granites are complexly associated with basic and ultrabasic intrusive rocks (bu), and both lithologies are in part overlain by the Wajid sandstone (€Ow); thus, the margins of most of the individual rock units are not easily defined spectrally. The calc-alkalic granites (gr) are equally well-defined spatially, but they cannot be visually distinguished from the peralkalic intrusions on the enhanced imagery. Overstreet and Rossman mapping at 1:100,000 scale (Reference 3) described both units as biotite granites, but noted that those corresponding to the (gr) tended to be porphyritic. This characteristic

Figure 6. Contrast-enhanced, ratio color-composite image of the Wadi Wassat area (digital scanner data from Landsat scene 1226-07011).

10

Figure 7. Geologic map of test area (modified after Reference 9).

PALEOZOIC

-€Ow   WAJID SANDSTONE   A — · — · A'   METASEDIMENT-METAVOLCANIC
                                                   SPECTRAL CONTACT

PERCAMBRIAN

gp	PERALKALIC GRANITE	a	AMPHIBOLITE
gr	CALC-ALKALIC GRANITE	sb	SCHISTOSE COMPLEX (ANDESITIC,
gg	GNEISSIC GRANITE		DIABASIC (AND LOCALLY DIORITIC)
d	DIORITE	sc	SCHIST (CHLORITE-SERICITE)
bu	ULTRABASIC INTRUSIVES	sl	SLATE
::::	GOSSAN AREA (WASSAT, QATAN,NEW)	(Tj)	TRONDHJEMITE (AFTER GREENWOOD)

———— —— —— IMAGE AREA FOR PRINCIPAL COMPONENTS AND CANONICAL ANALYSIS

11

is also described by Greenwood.* The spectral signatures would therefore be expected to be similar, and in fact, they are. The muscovite granite noted earlier on the black-and-white ratio images was not shown in the Asir Quadrangle even though intrusions of similar size had been mapped. This subtriangular intrusion, which is bluish-black on the ratio-composite image, was mapped by Greenwood and described as a muscovite granite. In addition to the excellent spectral correlation that exists with the granite intrusions, many other equally good correlations can be made. For example, schistose diabase (sb) is clearly defined as light greenish-blue hues at the southwestern image margin. The amphibolite (a) that intrudes the granite just west of image center is pinkish-buff on the enhanced imagery, whereas diorite (d) shows up as bluish-green hue. The purple spectral unit at image center corresponds to diorite intruded by felsic dikes on the Asir Quadrangle. Gneissic granite (gg) situated in the southwest quadrant rant appears as a dark-green hue. All of these rock units defined on the 1:500,000 geologic map correspond exceptionally well spatially, as well as spectrally, over the area.

Although the rock units mapped as schists (sc) at 1:500,000 also have good spatial correspondence to the ratio-composite image, they are made up of three locally distinctive spectral units. In addition, the slate (sl) comprising the host rock for the two western circular intrusions on the same map is also depicted as three discrete spectral units. In the case of both the schist and slate units, the three chromatically well-defined spectral units are pale green, cream, and finely mottled purple-blue and green. The most clearly defined spectral contact within the slate corresponds to the A-A' line on figure 7. Note that the pale-green units on the image also cannot be separated by visual inspection from the mapped ultrabasics on the basis of hue.

When these spectral units were compared with Greenwood's geologic maps, however, the lithologic relationships were immediately evident. All of the pale-green hues, including Brown and Jackson's (Reference 9) ultrabasics, coincided with mapped metamorphosed volcanic rocks. On the other hand, the off-white hues corresponded to metamorphosed sedimentary rocks, and the mottled units are described as metavolcanics intruded by diabase sills. Therefore, the A-A' line marks the contact between metasediments and metavolcanics. The well-defined purple unit, which was noted earlier to correspond with a diorite intruded by felsic dikes, was remapped by Greenwood as gabbro; the spatial distribution of this gabbro remained the same. The granites just west of the north arrow (N) designation on figure 7 (gg and gp) are shown as a dark-green hue. Greenwood mapped these intrusions as quartz monzonites.

A similar dark-green color dominates the gg unit mapped in the southwest corner of the image and is slightly lighter than the (Tj) unit. Greenwood shows this area (gg) to consist largely of trondhjomite and quartz diorite. As noted earlier, Precambrian terrain is locally overlain by the Wajid sandstone (€Ow). These isolated units are spectrally defined by several shades

*W. R. Greenwood, Reconnaissance geology of the Wadi Malaha and the Wadi Wassat quadrangles, Kingdom of Saudi Arabia, Scale 1:100,000 (in press).

of distinctive salmon-pink. The gossans that are developed above the massive sulphide deposits were too restricted to be included on the small-scale regional geological map. Both the Wadi Wassat and Wadi Qatan gossans, however, were mapped by Overstreet and Rossman (Reference 3).
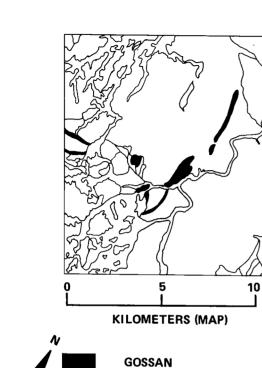
The Wadi Wassat gossans (W on figure 7) can be clearly identified on the ratio-color-composite image by their distinctive orange-red hue. However, the enhancement suggests that the gossans extend considerably further to the southwest than mapped by Overstreet and Rossman (Reference 3), and that they are commonly found adjacent on the north of a large granite intrusion. This could indicate that the gossans were incompletely mapped in the field, and Greenwood* shows this to be the case. The Wadi Wassat gossan, however, appears to be even more extensive than mapped by Greenwood. This wider dissemination of gossan material could very likely have been caused by fluvial action and/or gravity-induced mass movement. Note that, even though the gossans can be clearly identified using multispectral satellite data, their existence cannot be readily determined on standard black-and-white aircraft photographs at 1:60,000 scale (figure 8).

The Qatan area gossans (Q on figure 7), located about 15 kilometers southwest of the Wadi Wassat deposits, are shown by Overstreet and Rossman (Reference 3) to follow the strike of the local folding and to be very thin and discontinuous. Although some transported and re-deposited gossan material has been recognized locally in association with the Qatan gossans, Weissenborn and Earhart (Reference 2) found such detrital deposits to be less extensive than at the Wadi Wassat. This conclusion is confirmed by the ratio-color-composite Landsat image, because the Qatan gossans are much more restricted areally and can only be identified with difficulty. The characteristic red-orange lines, however, are so thin that they would probably have been overlooked on the imagery if their existence had not been previously known.

Approximately 7 kilometers southeast of the southern-most Qatan gossans, there is a well-defined orange-red hue (N on figure 7) on the enhanced image that suggests the presence of the largest single gossan within the area of the enhancement. Overstreet and Rossman (Reference 3) did not identify gossan material in this area, but its existence was later con-firmed by Dodge and Rossman (Reference 4) and by Greenwood* when the Wadi Wassat quadrangle was remapped.

It is readily apparent that, although some spectral ambiguities can be found when the enhanced imagery is compared with the earlier published maps, these discrepancies were largely resolved when the geology was more completely understood. Had the enhanced Landsat imagery been available to complement the early mapping efforts, the initial interpretations would

---

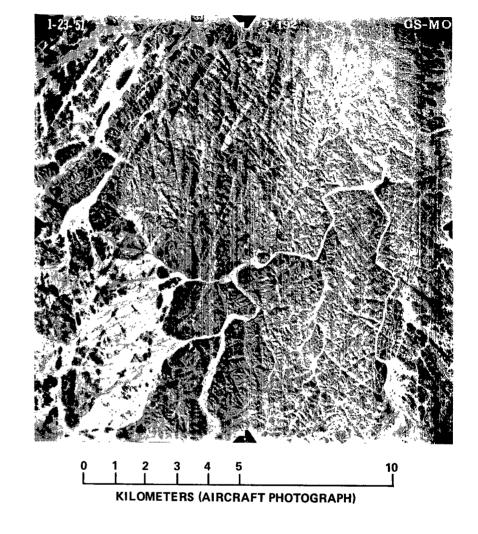*W. R. Greenwood, Reconnaissance geology of the Wadi Malaha and the Wadi Wassat quadrangles, Kingdom of Saudi Arabia, Scale 1:100,000 (in press).

KILOMETERS (MAP)

N

GOSSAN

FROM: PRELIMINARY GEOLOGIC MAP
WADI WASSAT QUADRANGLE
(GREENWOOD)

KILOMETERS (AIRCRAFT PHOTOGRAPH)

Figure 8. Wadi Wassat Gossan. Note that the gossan mapped by Greenwood is very poorly defined on a
standard black-and-white, low-altitude aerial photograph.

have undoubtedly been more complete (Brown, private communication, 1976). This image, in concert with a similarly enhanced scene to the south, has in fact contributed to resolving a regional stratigraphic correlation problem. The Magzah quadrangle immediately south of the Malahah quadrangle was independently mapped at 1:100,000 scale, and extreme difficulty had been encountered in joining the complex geology between the two. The most severe correlation problem was solved when the enhanced imagery showed that the metasedimentary rocks that extend south from the eastern most of the three small, circular intrusions (shown as an off-white hue on the ratio-composite image) continued southward as a discrete unit for a distance of more than 50 kilometers. Subsequent field work confirmed this finding, and, in addition, confirmed the existence of several previously unknown gossans that were first identified on the computer-enhanced imagery (Greenwood, private communication, 1976).

STATISTICALLY BASED PROCESSING

Next in this effort to evaluate computer capabilities for discriminating among rock classes involved evaluating several algorithms on the Pennsylvania State University ORSER System. Emphasis was placed on algorithms for principal-components analysis and for canonical analysis.

Principal-Components Processing

Principal-components analysis has been used for many years in various applications in statistics and biometrics; explanations of the statistical basis for the procedure may be found in numerous texts and journal articles. Applications to remote sensing have been presented previously by Podwysocki et al. (Reference 10), Williams and Borden (Reference 11), and Merembeck et al. (Reference 12).

Typically, the four original Landsat MSS bands are highly correlated (i.e., there is considerable redundancy in their information content). Principal-components processing is a procedure that determines a linear transformation that can condense the scene variance in the original data into a new set of variables (axes or principal components) that are uncorrelated (orthogonal in the 4-dimension data space). In addition, the scene variance tends to be concentrated into fewer new variables that still contain all of the original variability of the bands; this dimensionality reduction is the usual reason for using principal-components analysis on multivariate data. After transformation, the data were contrast-enhanced using a linear-stretch algorithm. This combination of procedures increases the spectral discrimination capability among terrestrial materials beyond that which can be attained using standard MSS data.

15

As reported here, principal-components processing of the Landsat MSS data for the Wadi Wassat test area was done in two modes. Interband statistics (table 1) are generated first. Then the two modes of principal-components analysis are applied to the interband statistical data; the eigenvalues and transformations are derived from the variance/covariance matrix rather than from the correlation matrix (Reference 13), following an unpublished algorithm implemented on the ORSER System. In the first mode (4-4), all four of the Landsat MSS bands are used at the same time to compute the principal-components and transformation matrix (table 2A). In the second mode (2-2-2), the four Landsat MSS bands are used two at a time (MSS-4 and -5, MSS-5 and -6, and MSS-6 and -7) to compute the principal-components and the transformation matrices (table 2B).

A set of four images is created from the processing for the first mode—one image for each of the transformed data axes or components. Inspection of the images (figure 9) shows a decrease in the image quality that parallels the decrease in the amount of scene variance contained in each component (table 2A). Six images are produced from the data that were transformed by the processing for the second mode. Three of these represent the concentration of scene variance in the first principal component for each pair of bands, whereas the other three represent the residual variance for each pair (table 2B). Spectral separation of various rock and soil types may be seen in the various gray patterns in the images for component axes 2, 3, and 4 for the first mode (figure 9) and for second component axes in the second mode (figure 10).

The visual information content of each of the data sets can be significantly improved if the images are combined into a color-composite image (figures 11 and 12) as was previously done with the contrast-enhanced ratio data (figure 6). Note that the values in the transformation matrices for the first principal component (component 1 of table 2A and the first principal components of table 2B) consistently have the same sign; the image produced by the transformation looks like a wide-band panchromatic image.

The images processed using principal-components analysis in both modes clearly demonstrate the utility of the transformations. The transformed images produced by the first mode (4-4) show the Wadi Wassat massive sulfide deposits as several small white-to-gray areas on the second axis image (figure 9) and as a small pink area in the color composite (figure 11). These areas correspond to the gossan area (W) on the geologic map (figure 7). Comparison of the images mentioned both above and below with the standard Landsat images (figure 5) shows no indication of any of the gossan areas on the standard images. The images for the second mode (2-2-2) show the sulfide deposits as small white areas on MSS-4 and -5, axis 2 (figure 10), which is the first residual image (green and red bands), and as small red areas on the color composite (figure 12). The areas indicated to be the Wadi Wassat gossan (W) on both images show good correspondence. Although the new gossans (N, figure 7) are also clearly visible in figure 12, they are nearly indistinguishable from the unaltered rock in figure 11. The specific reason for this is not readily identified.

16

Table 1
Interband Statistics for a Portion of Landsat Image 1226-07011
(March 6, 1973), Wadi Wassat, Saudi Arabia*

MSS Channels	4	5	6	7
Mean	44.22	50.71	46.31	19.34
Standard Deviation	8.47	13.40	13.27	5.85
Variance/covariance matrix				
4	71.74			
5	107.63	179.52		
6	103.23	172.39	175.97	
7	43.51	73.45	71.67	34.23
Correlation matrix				
4	1.00			
5	0.95	1.00		
6	0.92	0.97	1.00	
7	0.88	0.94	0.92	1.00

*These statistics are based on all picture elements (pixels) in the area of interest (659 elements by 841 scan lines = 554,219 observations). The main diagonal or trace of the covariance matrix contains the variance of each MSS band; off-diagonal elements of the matrix indicate the correlation between bands. This is borne out in the analysis of the correlation matrix. The variance value along the trace for any given MSS band divided by the summation of the trace gives the variance accounted for by each MSS band. The main diagonal or trace of the covariance matrix is discussed further in table 2.

Table 2
Transformation Statistics for Two Different Modes of Principal-Components
Analysis of the Wadi Wassat Test Area*

Component	Computed Eigenvalues	Percent	Cumulative Percent	Transformation Matrix (MSS Channel)			
				4	5	6	7
A (4-4 mode)							
Axis 1	445.149	96.464	96.464	0.38400	0.63103	0.62114	0.26179
Axis 2	8.534	1.849	98.313	-0.77366	-0.16729	0.60055	0.11316
Axis 3	4.809	1.042	99.355	0.35816	-0.40285	0.47965	-0.69237
Axis 4	2.978	0.645	100.000	0.35456	-0.64151	0.15318	0.66279
B (2-2-2 mode)							
MSS-4−5, axis 1	245.956	97.897	97.897	0.525	0.851	−	−
MSS-4−5, axis 2	5.284	2.103	100.000	-0.851	0.525	−	−
MSS-5−6, axis 1	350.158	98.498	98.498	−	0.711	0.704	−
MSS-5−6, axis 2	5.341	1.502	100.000	−	-0.704	0.711	−
MSS-6−7, axis 1	205.918	97.949	97.949	−	−	0.923	0.385
MSS-6−7, axis 2	4.312	2.051	100.000	−	−	-0.385	0.923

*In A, the computed eigenvalues are contained in the equivalence of the variance/covariance matrix after transformation; the eigenvalues are the main diagonal or trace elements of the matrix, and all off-diagonal elements are zero. Note that the summations of the eigenvalues in this table and the trace of the covariance matrix in table 1 are equal; thus, the scene variance is preserved. Note also that the eigenvalues are now in decreasing value, and the contribution of any one given axis can be calculated as explained in table 1. The new variables (e.g., component 1) are created by multiplying each of the transformation values of the row by its respective band and by summing that value. A contrast enhancement is then performed on these transformed data. In B, cumulative percent and pertinent associated values should be considered two at a time. See text for further explanation.

AXIS 1
96.464%

AXIS 2
1.849%

AXIS 3
1.042%

AXIS 4
0.645%

0   10   20
KILOMETERS

N

Figure 9. Principal-components analysis of the Wadi Wassat test area. Data were transformed using the (4-4) mode; scene variance is indicated for each image.

19

MSS-4 & 5, (5 & 6, AND 6 & 7
AXIS 1 SIMILAR)
97.897% (98.498 & 97.949)

MSS-4 & 5, AXIS 2
2.103%

MSS-5 & 6, AXIS 2
1.502%

MSS-6 & 7, AXIS 2
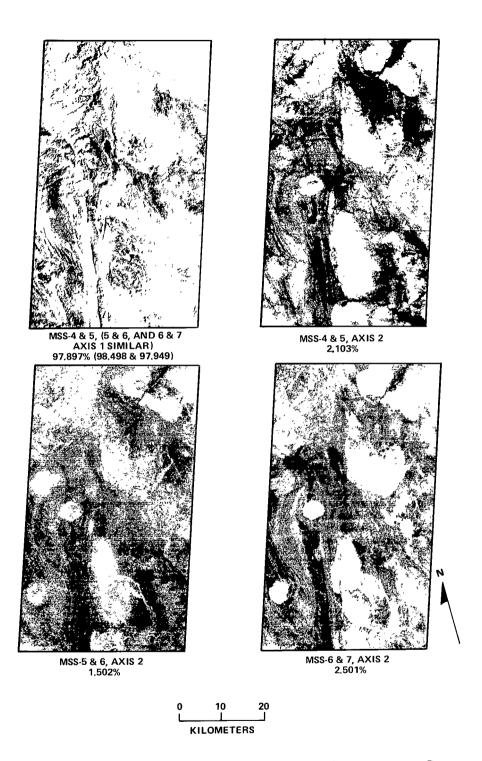2.501%

0   10   20
L____I____I
KILOMETERS

Figure 10.   Principal-components analysis of the Wadi Wassat test area. Data were transformed using the (2-2-2) mode; scene variance is indicated for each image.

Figure 11. Principal-components color-composite image of the Wadi Wassat test area based on digital MSS Landsat data transformed using the first (4-4) mode. This image was constructed using components 1, 2, and 3 projected through blue, red, and green filters, respectively; in this case, the third axis was printed through the green filter as a negative print.

21

0   10   20

KILOMETERS

Figure 12. Principal-components color-composite image of the Wadi Wassat test area based on digital MSS Landsat data transformed using the (2-2-2) mode. The second component of the MSS-4 and -5 transformation was projected through a red filter, MSS-5 and -6 through a blue filter, and MSS-6 and -7 through a green filter.

Examination of the transformation matrix in table 2 shows the relative importance of the individual Landsat bands for discriminating the gossan. For mode 1, axis 2 is interpreted as a contrast between the green band (MSS-4) and the first infrared band (MSS-6) with only a minor contribution from MSS-5 and -7. Because iron-rich materials with a red color tend to have a strong shoulder in their spectral curves between the red and green portions of the spectrum as opposed to nonred rocks, ratios such as those of MSS-4/5 tend to be very low for iron-rich areas. Rowan et al. (Reference 6) have shown that the MSS-4/6 ratio serves nearly the same purpose, particularly when there is some vegetation to confuse the interpretation. Conversely, in a MSS-5/4 or MSS-6/4 ratio, iron-rich areas would show as high ratios (bright areas in image format). The increased enhancement of the gossans that occurs when axis 3 of the color composite is printed as a negative print results from the summation of trans-formed values for reflectances in MSS-4. For mode 2, the first residual image is formed from MSS-4 and -5 only. The high negative loading for MSS-4 in each transformation matrix indicates that the low reflectance values of the pixels that represent the gossan are trans-formed to high values; thus, principal-components processing enhances a gossan in a manner similar to that of band-ratio processing. From these interpretations, it appears that Landsat MSS-4 (green band) is most significant in the detection of gossans.

Canonical Analysis Processing

Canonical analysis, like principal-components analysis, is used in digital image processing to produce an enhanced image by transformating multispectral data. The basic statistical data used in principal-components analysis are derived from the entire scene of interest—in this case, a part of a Landsat image. In contrast, the data used in canonical analysis come from selected small areas (training areas) of special interest within the image. Canonical analysis therefore maximizes the separation in spectral space among selected training areas and minimizes separation within the same group (References 10, 12, and 14). For this analysis, each training area was chosen for its spectral uniformity and was presumed to represent the spectral signature of a particular geologic material.

The first step in canonical analysis of the Wadi Wassat test site was the production of a reasonably complete classification map. Areas of spectral uniformity were identified using appropriate algorithms on the ORSER system and then thematically identified using the published and unpublished geologic maps. A sample of pixels (training area) was then selected from each uniform area to provide interband statistics for each category; the sample size was adjusted as necessary to minimize the variance within the category. Interim col-lections of category statistics were tested for spectral duplication by preliminary canonical analysis; redundant categories were merged or pruned. Interim classification mapping was then performed to locate additional areas within the test site that had not been mapped. The processes of selecting training areas and testing them with preliminary canonical analysis and classification mapping were repeated as necessary until most of the test site was mapped. At this stage, most of the large spectrally distinct areas had been accounted for; the procedures

resulted in numerous thematic categories (table 3) and spectral statistics (band and interband) that were provided as input to the canonical analysis procedure.

Images produced by canonical analysis (figure 13) clearly show the presence of the gossans. The Wadi Wassat gossans (W on figure 7) are seen as a series of light-gray patches in the image for axis 2. The same areas appear medium to dark gray in the image of axis 3, but they cannot be distinguished in the images of axes 1 and 4. In the color-composite image made using axes 1, 2, and 3 (figure 14), the Wadi Wassat gossans are shown as small reddish-purple areas. The geologic outcrop patterns interpreted from the combined images appear to be intermediate between the general areal pattern indicated by Brown and Jackson (Reference 9), and the detailed outcrop pattern shown by Greenwood;* the patterns are much closer in shape, location, and orientation to those mapped by Greenwood, but generally appear to be larger in size and to have gradational boundaries. The Wadi Wassat gossans stand out in strong spectral contrast in the images transformed by canonical analysis (gray tone on figure 13 or color on figure 14).

The Qatan and New gossans, as mapped by Greenwood,* do not show up as well as the Wadi Wassat gossans in the transformed images. The spectral signatures of these gossans must therefore be different from those of the Wadi Wassat gossan, which was used as the training site for the "gossan" signature (table 3). Examination of the figure 13 image set shows no distinct light-gray patches on axis 2 or dark-gray patches on axis 3 that correspond to the Qatan gossan as mapped by Greenwood,* nor do any equivalent color patterns show up on the color composite image (figure 14). The New gossan can also be seen in the images (figure 13) as a diffuse light-gray area on axis 2 and as a diffuse dark-gray area on axis 3; on the color composite of the images (figure 14), it appears as a purplish to reddish-purple area with very indefinite boundaries. However, note that, in the same image (figure 14), numerous areas are reddish or pinkish where it is known from detailed field mapping that the gossans do not occur. This makes it difficult to find the gossans solely by photointerpretation.

The statistical results of canonical analysis processing (table 4) show the relationships between the original channels and the transformed axes. The first axis accounts for most of the among-category variation (94.38 percent). The transformation matrix also shows all four of the MSS channels with positive loadings on axis 1, and the image representing axis 1 approximates a wide-band black-and-white photograph in a manner similar to that of principal-components analysis. Axis 2 is interpreted as a contrast between MSS-4 (green) and MSS-7 (near infrared) because the signs of the respective transformation elements are different and the absolute values of the elements are high. Axis 3 is interpreted as a contrast between MSS-4 plus MSS-7 against MSS-5. The high correlation between all channels and axis 1 indicates that all channels are necessary for making lithologic discriminations of this site (Reference 12).

*W. R. Greenwood, Reconnaissance geology of the Wadi Malaha and the Wadi Wassat quadrangles, Kingdom of Saudi Arabia, Scale 1:100,000 (in press).

24

Table 3
Spectral Signatures for Thematic Groups of Pixels*

Category	Theme Code	Spectral Average per Channel			
		4	5	6	7
1	QDS Aeolian Sand-1	60.0298	88.5821	85.3433	36.2239
2	QDS Aeolian Sand-2	64.2847	85.7810	80.3285	33.7299
3	Alluvium - 1	42.3333	44.9444	39.7778	15.8333
4	Gossan	43.1250	51.5000	47.6250	18.6250
5	Granite	42.3158	47.0526	42.5789	16.6316
6	Metasediments 1	42.4000	45.7000	40.0500	16.7500
7	Metasediments 2	64.2000	86.0286	81.1571	34.5714
8	Alluvium 2	66.0000	88.6889	83.6889	35.6222
9	Granite	70.6500	92.3750	86.8250	37.2500
10	Alluvium 3	69.8088	92.5294	86.4265	37.6176
11	Granite Alluvium	67.1739	88.6956	83.3913	35.3478
12	JDW Basalt-Andesite	40.5333	43.1333	37.7333	15.3333
13	JD 2 (shadow)	38.2115	39.0577	34.0961	13.7885
14	Dark Wadi Alluvium	54.0400	65.3600	62.6000	26.8400
15	DI Biotite Diorite	48.6000	54.2333	47.2667	18.9667
16	GMB Biotite Quartz Monzonite	39.6667	43.4444	39.8333	17.3333
17	QAL Wadi Alluvium	59.9512	75.2683	71.2195	30.3658
18	GB Olivine Gabbro	38.4000	41.0941	36.0588	14.7059
19	GMR Quartz Monzonite	39.4224	45.3535	42.2845	18.5345
20	GMRC Coarse Quartz Monzonite	46.2174	56.8261	52.1304	21.9565
21	QDS Aeolian Sand-3	58.1667	65.7719	59.1491	23.7105
22	QDS Aeolian Sand-4	62.3333	93.5000	88.2500	37.9167
23	QDS Aeolian Sand-5	63.8053	81.6549	74.5398	31.1947
24	JDQF Biotite Granofels	43.6533	49.2667	44.3333	18.2800
25	FD Felsic Dikes	47.6842	58.2105	52.2632	21.9474
26	DCW Wajid Sandstone (Q)	40.1905	44.1190	39.5238	16.3810
27	DCW Wajid Sandstone (QA)	33.3556	35.3333	31.9111	13.7333
28	JDQG-1 Graphitic Metasediments	36.8864	38.3409	35.5909	15.7273
29	JDQG-2 Graphitic Metasediments	34.0278	33.8472	30.1389	12.7361
30	QAL (dark) Alluvium	49.3613	57.3936	52.1871	21.2968
31	QAL Alluvium	61.2973	69.5676	66.0811	28.1351

*Multiple examples of the same theme represent spectral differences attributable to differences in ground slope or in source material. This is the input to classification mapping algorithms and part of the input to the canonical analysis algorithm.

AXIS 1
94.38 %

AXIS 2
4.85 %

AXIS 3
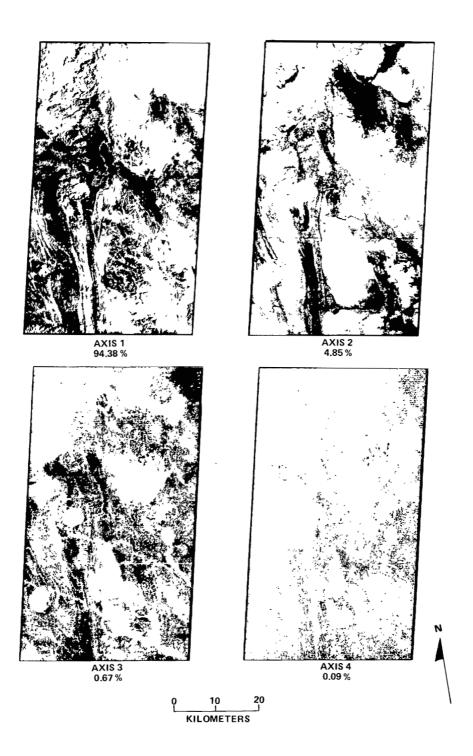0.67 %

AXIS 4
0.09 %

N

0   10   20
KILOMETERS

Figure 13.   Canonical analysis of the Wadi Wassat test area. Between categories
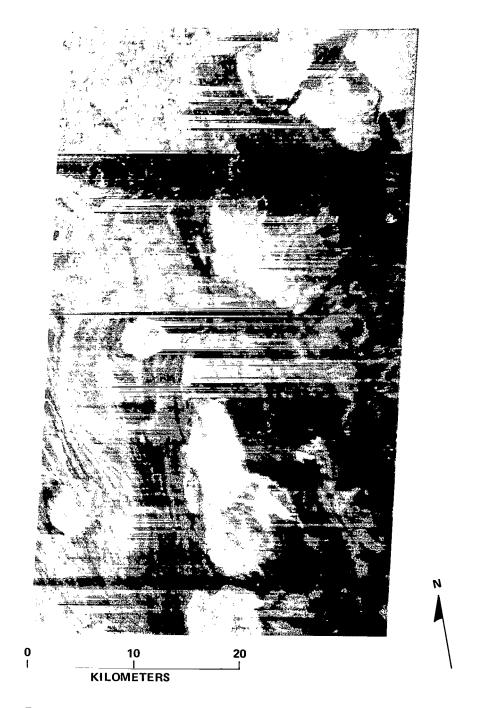(discriminatory) variance is indicated for each axis.

Figure 14. Canonical analysis color-composite image of the Wadi Wassat test area. Data from axes 1, 2, and 3 were projected through blue, red, and green filters, respectively.

Table 4

Canonical Analysis Statistics for the Wadi Wassat Test Area

Channel / Channel	Among Categories Covariance Matrix			
	4	5	6	7
4	230,000			
5	380,000	650,000		
6	370,000	630,000	620,000	
7	160,000	270,000	270,000	120,000

Channel / Channel	Pooled Within Categories Covariance Matrix			
	4	5	6	7
4	2.80			
5	2.30	5.10		
6	2.10	3.40	5.10	
7	0.94	1.60	1.60	1.20

Channel / Axis	Transformation Matrix (C)			
	4	5	6	7
1	0.08	0.20	0.18	0.16
2	-0.71	0.01	0.17	0.58
3	0.31	-0.54	-0.06	1.01
4	-0.04	0.38	-0.60	0.55

Channel / Axis	Correlations Between Channels and Axes			
	4	5	6	7
1	0.72	0.91	0.89	0.79
2	-0.65	-0.04	0.14	0.28
3	0.26	-0.28	0.02	0.48
4	0.00	0.29	-0.44	0.26

	Eigenvalues for (W EXP-1/2) * A * (W FXP-1/2)			
Axis	1	2	3	4
Variance	150,000	7,800	1,100	1.50
Percent of Total	94.38	4.85	0.67	0.09

Channels used: 1 2 3 4
Number of categories: 31
Total number of observations: 1648

ROCK CLASSES

In addition to using enhanced Landsat images to more effectively locate gossans in the test site than could be accomplished by using standard Landsat images, the general rock discrimination capability of the enhanced images was also tested.

Brightness differences permit the same boundaries to be drawn on standard Landsat images (figure 5) and on any of the first-order images of transformed data (axis 1 of canonical analysis on figure 13, axis 1 of principal-components analysis, 4-4 mode, on figure 9, and/or axes 1 of the MSS-4 and -5, MSS-5 and -6, and MSS-6 and -7 transformation using principal-components analysis in the 2-2-2 mode, on figure 10). Although bedrock can be readily distinguished from alluvium and dune sands on any of these images, it is not easy to distinguish among the various Precambrian bedrock lithologies or between dune sands and alluvial materials.

Considerable success in the discrimination of rock units, however, can be obtained by examining images made by using the various higher-order transformed data. These images frequently display spectral variation among rock types that is not expressed in the brightness information of standard Landsat photographs or first-order images. Distinctions can be made among several Quaternary deposits using the enhanced (both ratio and transformed) images; in the northeast corner of the transformed images, for example, there is a strong spectral contrast between dune sands and alluvium (figures 9, 10, and 13). In addition, many wadis show spectral reflectivity changes either along their length or from one branch to another; this suggests the capability of identifying differences in source material for certain alluvial deposits. A comparison of higher-order transformed images with first-order images and/or standard Landsat images (figure 5) and with geologic maps supports the hypothesis that much of the alluvium in the test area displays spectral reflectivities similar to nearby bedrock areas. In other areas, outcrops of the Wajid Sandstone can be detected by gray-level differences in the higher-order transformed images, but this stratigraphic unit cannot be discriminated everywhere that it has been mapped in the field.* Certain small granite intrusions are also very distinct. (Compare images with figure 7.) In other cases, lithologic distinctions shown on the geologic map are difficult to see on the enhanced imagery. In almost all images, standard or enhanced, the contacts of the intrusive units are well-defined. This is due primarily to their surface geometry and locally to changes in surface texture.

The images made by using the various statistical transformations cross only a small portion of line A-A' (figure 7) that separates two very distinct spectral units that were mapped as a single slate unit (Reference 9). At best, the transformed images show only a slight difference in color on each side of the boundary (figure 14). This distinction is adequate, however, to suggest that the A-A' line would also be defined on the various transformed images if they had covered more area to the west.

---

*W. R. Greenwood, Reconnaissance geology of the Wadi Malaha and the Wadi Wassat quadrangles, Kingdom of Saudi Arabia, Scale 1:100,000 (in press).

On most of the transformed images (figures 9, 10, and 13) showing single-axis data, no distinction exists in gray tone among the small, circular, granitic intrusives mapped as "gp" (figure 7). In the residual image for the principal-components analysis (2-2-2 mode) using MSS-4 and MSS-5 as input, however, a considerable difference exists in gray tone between two of the intrusives. (See figure 10, and compare axis 2 with other images.) A similar difference in gray tone may be seen in the second axis of the 4-4 mode of principal-components transformation (figure 8); this axis is essentially a contrast between MSS-4 and MSS-6. Although they appear to be different spectral rock types, these two intrusives were mapped as a single unit by Greenwood* at a scale of 1:100,000.

In the southeastern corner of the reconnaissance map (figure 7), three areas are mapped as "gr." On almost all enhanced transformed-data images, these bodies differ in gray levels. The difference is especially striking in the color composites for the canonical transformation (figure 14). On the standard Landsat images (figure 5), the three units appear to have essentially the same tone.

The various transformed-data image enhancements provided imagery that permitted the discrimination of rock units in greater detail than could be accomplished using standard Landsat images, and they provided more geologic information than is generally included on small-scale (1:500,000) reconnaissance geologic maps.

COMPARISON OF ENHANCED IMAGES

A qualitative comparison of the geologic information contained in each of the enhanced images showed that the contrast-stretched ratio color-composite image permitted the best overall visual identification of lithology and alteration products. The wider range of colors within this image permitted discrimination among a considerably larger group of rock classes; conversely, fewer ambiguities occurred in identification. This greater chromatic range may have been caused by the different contrast-stretch algorithms envoked by the different processing techniques. The ratio-stretch algorithms can also be used to process data in a single operation for a larger scene area. This provides the wider field of view that is so valuable for many regional studies. The principal-components and canonical-analysis algorithms can provide the same area coverage by combining several processed subscenes, but this requires additional time and costs. On the other hand, the stretched-ratio procedures do not permit the acquisition of interband statistics for quantitative studies.

Images produced by canonical analysis have two advantages over those produced by principal-component analyses: (1) the color-composite images show greater color separation among the various rock units, and (2) preprocessing permits the generation of statistical data for

---

*W. R. Greenwood, Reconnaissance geology of the Wadi Malaha and the Wadi Wassat quadrangles, Kingdom of Saudi Arabia, Scale 1:100,000 (in press).

selected areas within the study area. These data can then be used for classification mapping and statistical comparisons between the selected training areas. However, principal-components analysis is much less expensive and still contains much of the same statistical information. The use of total scene variance in the principal-components processing rather than variance among selected samples, however, retains some random noise in the lower-order transformed images.

Each of the three differently enhanced Landsat images provided unique enhancement parameters for identifying specific materials in the study area, and all provided significantly better identification of surface geology than could be accomplished using standard Landsat images.

SUMMARY AND CONCLUSIONS

The results of this investigation appear to represent significant progress toward solving the long-standing problem of rock identification by remote sensing from space. This problem is caused in part by the inherent resolution loss of orbital sensing and in part from the fact that existing Landsat data are obtained only for reflected radiation in the visible and near-infrared part of the electromagnetic spectrum. However, this document shows that computer-enhancement programs can process digital Landsat MSS data so that they contribute to meaningful discrimination of rock and rock-alteration materials.

The most useful product for visual interpretation has been a color-composite image constructed by using contrast-stretched ratio data. Using this imagery, it was possible to visually discriminate among a wide variety of igneous and metamorphic rock classes and to identify gossans overlying known massive sulphide deposits. Spectral correspondence to rock units mapped at a scale of 1:100,000 appeared visually to be greater than 80 percent. Color-composite enhanced imagery constructed by using principal-components and canonical-analysis algorithms permitted visual separation of several major rock units, but the inherent more narrow range of color variation caused ambiguity in distinguishing among some of the rock classes that could be easily defined on the ratio image. However, both transformation algorithms generated interband statistics that can be used in further quantitative studies.

All classes of enhanced imagery considered here corresponded considerably better to the largest scale geologic maps than the standard Landsat imagery did.

The area selected for this study was admittedly selected for the variety and extensiveness of its rock outcrops, negligible vegetation, and minimal soil and chemical weathering cover. However, it is hoped that, with modification and improvements in digital enhancement/transformation techniques and/or sensors carried on future satellites, the general techniques discussed will be equally applicable in other, more humid regions.

ACKNOWLEDGMENTS

The authors sincerely thank G. F. Brown, W. R. Greenwood, D. G. Hadley, and T. H. Kiilsgaard for providing unpublished maps and field data and for invaluable discussions. A valid geological interpretation of the enhanced Landsat imagery would not have been possible without their generous cooperation. W. C. Shoup processed the contrast-stretched ratio imagery, and L. V. Maness, Jr., provided technical support for part of the principal-components and canonical-analysis processing. K. T. Meehan, A. T. Watson, and P. D. Lowman, Jr., kindly reviewed the manuscript.

REFERENCES

1. Jackaman, B., "Genetic and Environmental Factors Controlling the Formation of the Massive Sulphide Deposits of Wadi Bidah and Wadi Wassat, Saudi Arabia," Director General of Mineral Resources, Ministry of Petroleum and Mineral Resources, Technical Report TR-1972-1, 1972, 243 pp.

2. Weissenborn, A. E., and R. L. Earhart, "Appraisal of the Wadi Wassat and Wadi Abhbat Pyrite Deposits, Asir Quadrangle, Kingdom of Saudi Arabia," U.S. Geol. Survey Saudi Arabian Project Technical Letter 101, 1968, 21 pp.

3. Overstreet, W. C., and D. L. Rossman, "Reconnaissance Geology of the Wadi Wassat Quadrangle, Kingdom of Saudi Arabia," U.S. Geol. Survey Saudi Arabian Project Report 117, 1970, 68 pp.

4. Dodge, F. C. W., and D. L. Rossman, "Mineralization in the Wadi Qatan Area, Kingdom of Saudi Arabia," U.S. Geol. Survey Saudi Arabian Project Report 190, 1975, 71 pp.

5. Blodget, H. W., G. F. Brown, and J. G. Moik, "Geological Mapping Northwestern Saudi Arabia Using Landsat Multispectral Techniques," *Proceedings of the NASA Earth Resources Survey Symposium*, NASA TM X-58168, 1975, *JSC-09930, v. I-B*, pp. 971-990.

6. Rowan, L. C., P. H. Wetlaufer, A. F. H. Goetz, F. C. Billingsley, and J. H. Stewart, "Discrimination of Rock Types and Detection of Hydrothermally Altered Areas in Southcentral Nevada by the Use of Computer-Enhanced ERTS Images," U.S. Geol. Survey Prof. Paper 883, 1974, 35 pp.

7. Goetz, A. F. H., F. C. Fillingsley, A. R. Gillespie, M. J. Abrams, R. L. Squires, E. M. Shoemaker, I. Lucchitta, and D. P. Elston, "Applications of ERTS Images and Image Processing to Regional Geologic Problems and Geologic Mapping Northern Arizona," Technical Report 32-1597, Jet Propulsion Laboratory, Institute of Technology, Pasadena, California, 1975, 187 pp.

8. Estes, J. E., and D. S. Simonett, "Fundamentals of Image Interpretation," *Manual of Remote Sensing*, R. G. Reeves, ed., American Soc. of Photogrammetry, Falls Church, Virignia, 1975, pp. 869-1076.

9. Brown, G. F., and R. O. Jackson, "Geologic Map of the Asir Quadrangle, Kingdom of Saudi Arabia," U.S. Geol. Survey Map I-217A, Scale 1:500,000, 1959.

10. Podwysocki, M. H., F. J. Gunther, and H. W. Blodget, "Discrimination of Rock and Soil Types by Digital Analysis of Landsat Data," NASA TM X-71290, 1977, 37 pp.

11. Williams, D. L., and F. Y. Borden, "A Reduction in Ag./Residential Signature Conflict Using Principal Components Analysis of Landsat Temporal Data," NASA TM X-71387, 1977, 10 pp.

12. Merembeck, B. F., F. Y. Borden, M. H. Podwysocki, and D. N. Applegate, "Application of Canonical Analysis to Multispectral Scanner Data," *Proc. 14th Ann. Symp. on Computer Applications in the Mineral Industries*, University Park, Pennsylvania, September 1976.

13. Trochimczyk, J., and F. Chayes, "Some Properties of Principal Component Scores," *Mathematical Geology*, 10(1), 1978, pp. 43-51.

14. Seale, H. L., *Multivariate Statistical Analysis for Biologists*, Methuen & Co., London, 1964, 209 p.

BIBLIOGRAPHIC DATA SHEET

1. Report No. NASA TP-1327	2. Government Accession No.	3. Recipient's Catalog No.

4. Title and Subtitle Discrimination of Rock Classes and Alteration Products in Southwestern Saudi Arabia with Computer-Enhanced Landsat Data		5. Report Date October 1978
		6. Performing Organization Code 923

7. Author(s) H. W. Blodget, F. J. Gunther, and M. H. Podwysocki	8. Performing Organization Report No. G7802-F16

9. Performing Organization Name and Address Goddard Space Flight Center Greenbelt, Maryland 20771	10. Work Unit No. 177-54-43
	11. Contract or Grant No.

12. Sponsoring Agency Name and Address National Aeronautics and Space Administration Washington, D.C. 20546	13. Type of Report and Period Covered Technical Paper
	14. Sponsoring Agency Code

15. Supplementary Notes

16. Abstract

Digital Landsat MSS data for an area in the southwestern Arabian Shield have been computer-enhanced to improve discrimination of rock classes, and recognition of gossans associated with massive sulphide deposits.

The test area is underlain by metamorphic rocks that are locally intruded by granites; these are partly overlain by sandstones. The test area further includes the Wadi Wassat and Wadi Qatan massive sulphide deposits, which are commonly capped by gossans of ferric oxides, silica and carbonates.

Color patterns and boundaries on contrast-stretched ratio color composite imagery, and on complementary images constructed using principal component and canonical analyses transformations, correspond exceptionally well to 1:100,000 scale field maps. A qualitative visual comparison of information content showed that the ratio enhancement provided the best overall image for identification of rock type and alteration products.

17. Key Words (Selected by Author(s)) Earth Resources, Geology, Image Processing, Saudi Arabia, Band Ratioing, Principal Components Analysis, Canonical Analysis	18. Distribution Statement STAR Category 42 Unclassified—Unlimited		

19. Security Classif. (of this report) Unclassified	20. Security Classif. (of this page) Unclassified	21. No. of Pages 40	22. Price* $4.50

*For sale by the National Technical Information Service, Springfield, Virginia 22161.

National Aeronautics and
Space Administration

Washington, D.C.
20546

Official Business

Penalty f(

U.S.MAIL

1   1 1U, E,   092978 S00903DS
DEPT OF THE AIR FORCE
AF WEAPONS LABORATORY
ATTN: TECHNICAL LIBRARY (SUL)
KIRTLAND AFB NM 87117

NASA S